Available online at www.sciencedirect.com
SCIENCE DIRECT®
Journal of Nuclear Materials 350 (2006) 182–194
journal of nuclear materials
www.elsevier.com/locate/jnucmat

# Determining the shear properties of the PyC/SiC interface for a model TRISO fuel

T. Nozawa *, L.L. Snead, Y. Katoh, J.H. Miller, E. Lara-Curzio

*Metals and Ceramics Division, Oak Ridge National Laboratory, Oak Ridge, TN 37831, USA*

Received 26 September 2005; accepted 6 January 2006

**Abstract**

The fracture behavior of TRISO-coated fuel particles is dependent on the shear strength of the interface between the inner pyrolytic carbon (PyC) and silicon carbide coatings. This study evaluates the interfacial shear properties and the crack extension mechanism for TRISO-coated model tubes using a push-out technique. The interfacial debond shear strength was found to increase with increasing sample thickness and finally approached a constant value. The intrinsic interfacial debond shear strength of ~280 MPa was estimated. After the layer is debonded, the applied load is primarily transferred by interfacial friction. A non-linear shear-lag model predicts that the residual clamping stress at the interface is ~350 MPa, and the coefficient of friction is ~0.23, yielding a frictional stress of ~80 MPa. These relatively high values are attributed to the interfacial roughness. Of importance in these findings is that this unusually high interfacial strength could allow significant loads to be transferred between the inner PyC and SiC in application, potentially leading to failure of the SiC layer.


*PACS:* 68.35.Ct; 68.35.Gy; 81.05.Je; 81.70.Bt

## 1. Introduction

A future generation of nuclear fission energy systems, known as Generation IV (Gen IV), is being pursued for potential economic, safety, waste production, and proliferation resistance benefits [1]. Moreover, the very high temperature gas-cooled reactor (VHTR), a Gen IV candidate advanced reactor, has a potentially great advantage by coupling superior thermodynamic system cycle efficiency with the utilization of process heat for hydrogen production. To achieve its target reliability and performance, the VHTR and other Gen IV concepts rely on the performance of high quality coated particle fuel operating at very high temperature and high neutron dose.

The TRISO (TRIstructural ISOtropic) coating fuel system acts as a pressure vessel to contain internal gas pressures generated during fission of the kernel material and also as a diffusion barrier to

* Corresponding author. Tel.: +1 865 576 6301; fax: +1 865 241 3650.
*E-mail address:* nozawat@ornl.gov (T. Nozawa).

0022-3115/$ - see front matter 
doi:10.1016/j.jnucmat.2006.01.004

contain gaseous and metallic fission products [2,3]. The TRISO fuel particle is composed of the kernel of fission material and four functional overlayers: low-density buffer pyrolytic carbon (BPyC), high-density inner PyC (IPyC), silicon carbide (SiC) and high-density outer PyC (OPyC) (Fig. 1). The coated particle fuel is subjected to many forces that put stress on the TRISO coating. High density IPyC and SiC layers are impervious to fission gases at normal operating temperatures and the SiC layer primarily acts as a structural material. Potential failure mechanisms have been previously summarized [4]. For many of failure mechanisms, transmission of load across the IPyC (or OPyC) and the SiC is of fundamental importance and deserves detailed understanding.

Under neutron irradiation, anisotropic volume changes in the fuel kernel and/or the pyrolytic carbon often cause cracking within the IPyC layer that can penetrate through the SiC layer (Fig. 1(b)) or partial debonding at the IPyC/SiC interface (Fig. 1(c)). If the layers do not completely debond at once or if only partial debonding occurs, severe stress concentration occurs at the tip of the crack opening between layers, resulting in a finite probability of failure of the SiC layer. Miller et al. [5,6] have developed numerical models to predict the fuel performance based on these phenomena. In contrast, if the tensile radial stress that develops between the IPyC and the SiC layers during irradiation exceeds the bonding strength, then the layers would debond relieving stresses. If complete debonding occurs, the stress between IPyC and SiC is effectively zero. The SiC layer would no longer experience concentrated stresses associated with shrinkage cracks. This would decrease not only the probability that a shrinkage crack would lead to failure of the particle, but also the overall failure probability. In this case, the primary cause of stress in the SiC layer would be fission product gas buildup, limiting the failure to the more traditional pressure vessel failure mode. The complete debonding may increase the probability of the pressure vessel failure due to uniform pressurization, since the SiC stress due to pressure would increase with a debonded IPyC. The primary failure mechanism therefore significantly depends on the magnitude of the bonding strength between layers.

The experimental methods currently available for interfacial strength characterization of coated material are very limited and have been primarily developed by the ceramic composites community. Mini-composite tensile testing is one option to evaluate the interfacial shear properties of coated tubes [7]. However, there remains the difficulty of gripping very thin specimens while ensuring no bending

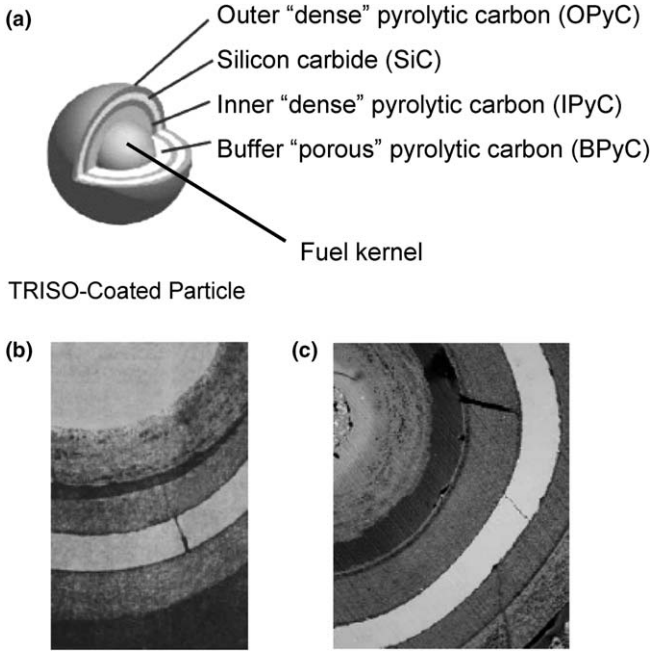


Fig. 1. (a) Schematic illustration of a TRISO-coated fuel particle, (b) and (c) typical micrograph after burnup [4].

moment is present, which would invalidate the test results. Additionally, it would be difficult to determine an actual crack path of multi-layered interface material, which may propagate at both the BPyC/IPyC and the IPyC/SiC interfaces. Currently, the only viable relevant tests for measuring the interfacial shear properties are the single fiber push-in and push-out tests, most widely used in the mechanical characterization of the fiber/matrix interface for the composite system [8–15].

Usually the push-in/-out tests have been performed by the nano-indentation technique [8,9]. However, as a result of the limited load capacity of the systems, such testing is restricted to evaluation of composites with a small diameter fiber. Moreover, a sharp indenter tip such as Vickers or Berkovich makes it difficult to analyze experimental data due to fiber deformation. They are therefore inadequate for low shear strength fibers such as carbon with onion structure [16]. For the same reason, utilization of the sharp indenter would be inadequate for the layered TRISO-coated model tube. Recently, a micro-indentation test system was developed for interfacial characterization of large diameter fiber composites [10]. According to this test method, the inner phase is pushed-out from the outer phase using a hard flat-bottomed punch and a universal testing machine. Parallel to the development of experimental methods and techniques to evaluate the interfacial properties, several numerical analyses have been developed and their applicability has been proven [9,17–26].

The objective of this study is to evaluate the interfacial shear properties and crack extension mechanism at the IPyC/SiC interface in a (non-irradiated) TRISO-coated model tubular test specimen using the micro-indentation push-out test technique. Specifically, this study aims to quantify the interfacial shear properties for modeling the fracture behavior of TRISO-coated fuel particles.

## 2. Experimental

### 2.1. Material

TRISO-coated model tubes were fabricated by chemical vapor deposition (CVD). Deposition conditions were the same as those used for actual fuel preparation [4]. A SCS-9A™ SiC fiber (Specialty Materials, Inc., Lowell, MA) with a diameter of 75 μm was used as a core material. A buffer pyrolytic carbon with a thickness of ~40 μm was chemically vapor deposited on 5 mm-long chopped SiC fibers with the source gas of acetylene ($C_2H_2$) in a gas flow of argon at 1300 °C. The density of BPyC is reportedly ~1 g/cm$^3$ [27–29]. An inner dense pyrolytic carbon with a thickness of ~23 μm was subsequently deposited around the BPyC layer with mixed gas sources of $C_2H_2$ and propylene ($C_3H_6$) in an argon gas flow at 1300 °C. The density of IPyC is ~2 g/cm$^3$ [27–30]. Both BPyC and IPyC are nearly isotropic with Bacon anisotropy factors (BAFs) reported to be 1.00 and 1.05, respectively [29,30]. The silicon carbide layer (~60 μm) was deposited using methyltrichlorosilane (MTS, Gelest Inc., Morrisville, PA) at 1500 °C with a hydrogen gas carrier. The resulting polycrystalline cubic CVD-SiC provides a density of ~3.2 g/cm$^3$.

TRISO-coated tubular samples were embedded in epoxy and sliced into three pieces. Slices were then polished to desired sample thickness ranging from 70 to 340 μm using standard metallographic techniques. Both surfaces of the specimens were polished to a surface finish of 5 μm. A subset of samples was polished to a surface finish of 1 μm for microstructural observation. Note that the interface remained good bonding regardless of the magnitude of the surface finish. A typical cross-sectional micrograph of a model tubular test specimen is shown in Fig. 2. Layered structures were successfully deposited around the SCS-9A™ SiC fiber core. The IPyC/SiC interface of model TRISO fuel appears to form a relatively tight bond because SiC is deposited onto the rough PyC layer. This structure is very similar to that of the actual TRISO fuel [4]. There are no serious machining flaws observed.

Major constituent properties are summarized in Table 1. The Young's modulus of each layer, which was determined by nano-indentation with a Berkovich type indenter tip following the method of Oliver [31], is also listed. This data exhibits good agreement with published data [27–30,32–38].

### 2.2. Push-out test

Push-out tests were performed using a micro-indentation test system. Fig. 3 shows a schematic illustration of the push-out system used in this study. The polished specimens were bonded by epoxy-based adhesive to a brass specimen holder over a ~230 μm diameter hole. They were then loaded with a conical tungsten carbide (WC) indenter with a

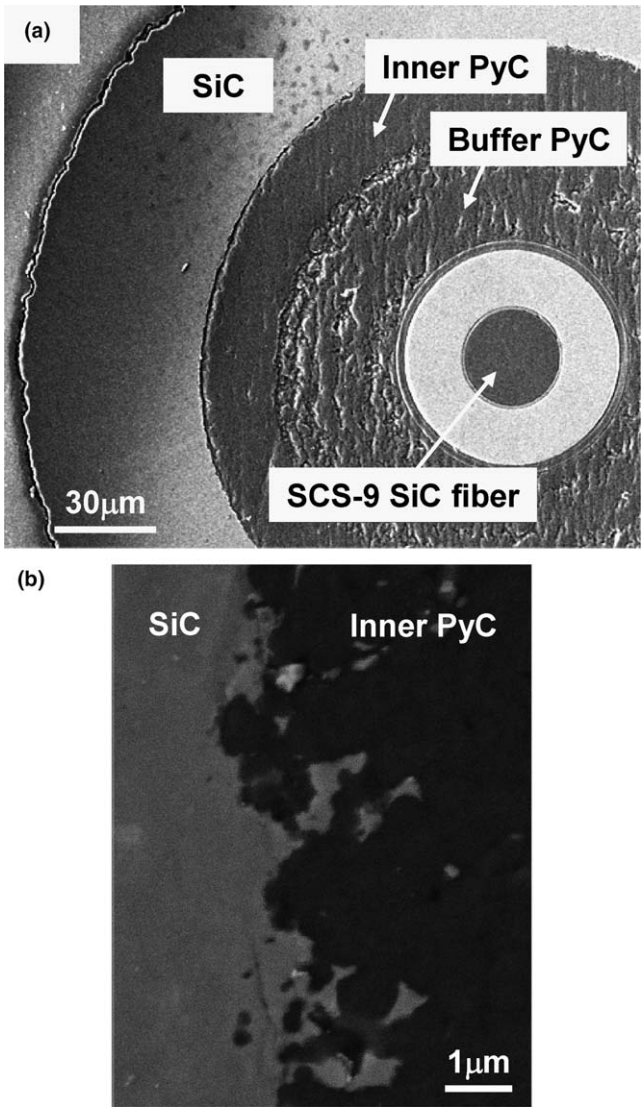


Fig. 2. Typical cross-sectional micrographs of TRISO-coated model tubes: (a) TRISO structure and (b) inner PyC/SiC interface.

flat-bottomed tip (195 μm in diameter). The cone angle was approximately 20°. An optical microscope was used to locate and load the specimen center. A 100 N capacity load cell was used to measure the applied load. The crosshead displacement rate was 20 μm/min and the indenter end displacement was measured by a laser extensometer. Some cyclic unloading/reloading tests were conducted to track crack initiation and propagation. The surface microstructure of the TRISO-coated model tubular test specimen was examined by optical microscopy and scanning electron microscopy.

## 3. Results

### 3.1. Push-out behavior

In most experiments, a push-out crack successfully propagated along the IPyC/SiC interface. However, some TRISO-coated model tubes failed in different modes: by bending or shear deformation (Fig. 4). These results suggest potentially strong interfacial shear strength at the IPyC/SiC interface of the TRISO-coating, although these experimental values were disregarded because the loading

Table 1
Material parameters of constituents of a TRISO-coated model tube

| Valuables | Value | Note/citation |
|---|---|---|
| *SCS-9A SiC fiber* | | |
| Elastic | 341 | Nano-indentation (this work) |
| modulus (GPa) | 307 | Product sheet from manufacturer [32] |
| Poisson's ratio | 0.2 | Assumed |
| *Buffer PyC* | | |
| Density (g/cm$^3$) | ~1 | Kaae [27–29] |
| BAF[a] | 1.00 | Kaae [29], Price and Bokros [30] |
| Elastic | 23 | Nano-indentation (this work) |
| modulus (GPa) | 11 | Kaae [33] |
| Poisson's ratio | 0.23 | Price and Kaae [34] |
| *Inner isotropic PyC* | | |
| Density (g/cm$^3$) | ~2 | Kaae [27–29], Price et al. [30] |
| BAF[a] | 1.05 | Kaae [29], Price et al. [30] |
| Elastic | 31 | Nano-indentation (this work) |
| modulus (GPa) | 26 | Kaae [33] |
| Poisson's ratio | 0.23 | Price and Kaae [34] |
| CTE[b] ($10^{-6}$/°C) | 3.5–5.1 | Price et al. [35] |
| CVD-SiC | | |
| Density (g/cm$^3$) | 3.21 | Product sheet from manufacturer [36] |
| Elastic | 440 | Nano-indentation (this work) |
| modulus (GPa) | 460 | Product sheet from manufacturer [36] |
| | 430 | Price [37] |
| Poisson's ratio | 0.21 | Product sheet from manufacturer [36] |
| | 0.13 | Yavuz and Tressler [38] |
| CTE[b] ($10^{-6}$/°C) | 4.0 | Product sheet from manufacturer [36] |
| | 4.9 | Price [37] |

[a] Bacon anisotropy factor.
[b] Coefficient of thermal expansion.

conditions were not valid. Fig. 4(a) exhibits a crack initiated by a bending moment deflected at the weak BPyC/IPyC interface and then propagating through the IPyC/SiC interface. In contrast, most of the thick specimens exhibited shear deformation of the weak PyC until the applied load overcame the complete debonding load (Fig. 4(b)).

Fig. 5 shows typical load/displacement curves obtained from push-out tests. These load/displacement curves could be classified in two groups: one group exhibits mostly linear load/displacement behavior, which was typical of thin test specimens (<200 μm), resulting in a load drop at the maximum load; the other group of curves exhibits non-linear load/displacement behavior beyond the proportional load limit followed by a load drop. The latter behavior was typical of thicker test specimens (>200 μm). As seen in the fracture surfaces of pushed-out specimens (Fig. 6), a large crack propagated between IPyC and SiC, and the inside core was successfully pushed-out. Beyond the load drop, most specimens for which SiC layer failure did not occur exhibited a plateau in the load–displacement. However, the plateau was limited, followed by a rapid load drop. As described in the discussion section, the second rapid load drop was associated with fracture of the SiC layer. Some radial cracks in the outer SiC layer were observed in pushed-out surfaces. Fig. 6 also shows some damage at the edges in the PyC layer. This might be induced by wearing at the interfacial friction.

The proportional limit in the load–displacement curve is typically associated with the initiation of

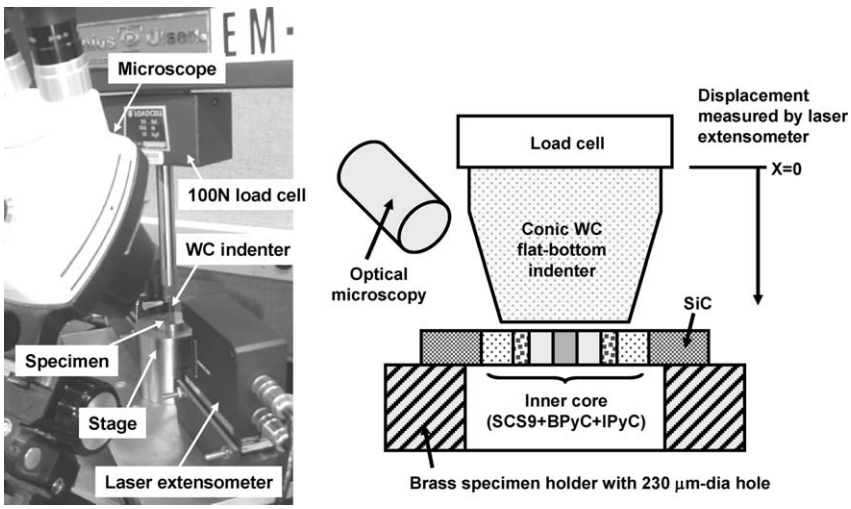


Fig. 3. Schematic illustration of the push-out test system.

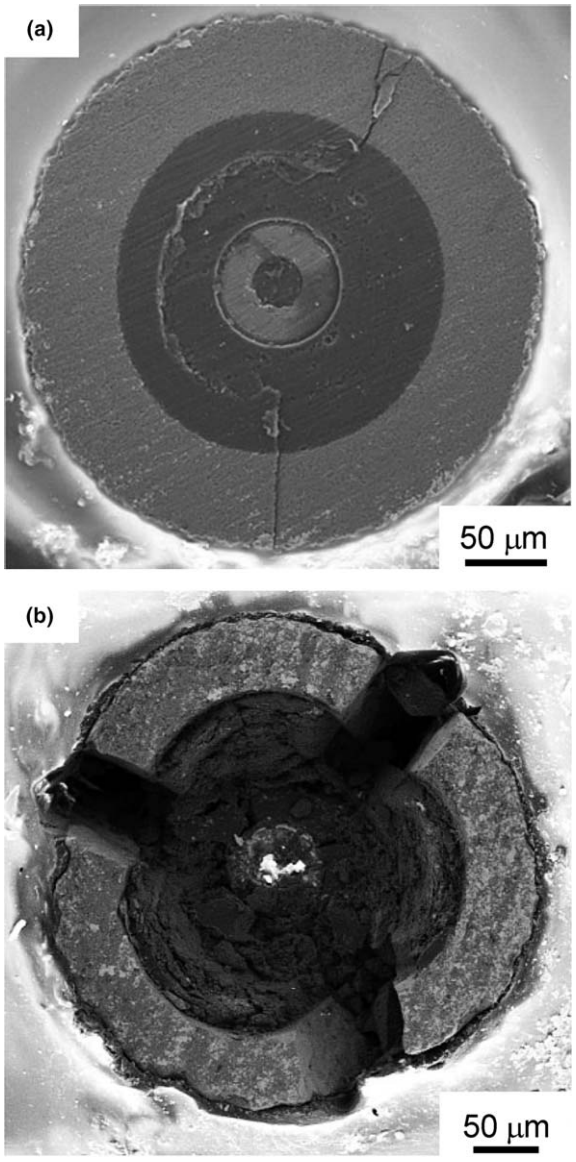


Fig. 4. Invalid fracture surfaces of TRISO-coated model tubes failed by (a) bending and (b) shear deformation of carbon.

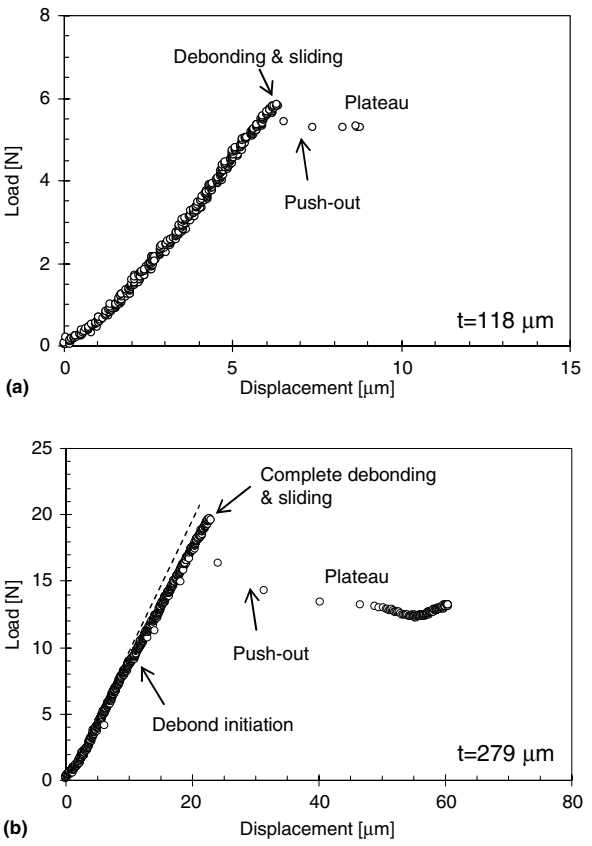


Fig. 5. Typical push-out load–displacement curves of TRISO-coated model tubes: (a) thin specimen (118 μm) and (b) thick specimen (279 μm).

an interfacial crack, i.e., interfacial debonding [10–12]. Fig. 7 shows separate loading/unloading curves and corresponding pushed-out surface images of the 330 μm-thick TRISO-coated model tube. The slight slope change detected around 12 N during the second loading segment corresponds with the debond initiation according to microstructural observations. A single large crack is formed along the IPyC/SiC interface above 12 N. The actual crack path did not follow the IPyC/SiC interface because of the roughness of the interface. The non-uniform deposition on the rough surfaced core tube resulted in a very tortuous crack path. From quantitative analysis of the micrographs, it is estimated that the interfacial roughness is of the order of several hundreds nanometers.

Fig. 7 also exhibits shear deformation of the PyC inner core, which was typical for very thick specimens, due to inherently weak shear strength of the PyC layer. However, shear deformation never occurred until the applied load reached a maximum value. This confirmed that the debond initiation was not associated with the initiation of shear deformation of PyC. In this study, debond initiation load is regarded as valid even if the model tubular specimen failed in shear.

Once the interface has debonded, the displacement of the core end is significantly enhanced and the load/displacement curves become non-linear. The non-linear segment results from mixed fracture processes which include progressive debonding ahead of the crack front and friction between the

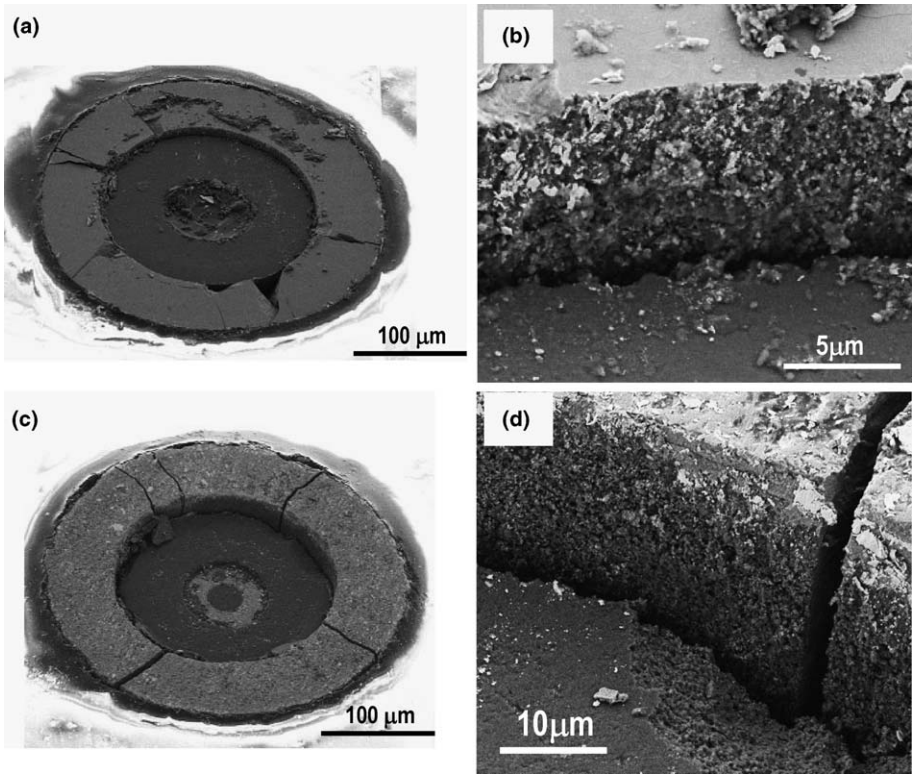


Fig. 6. Typical valid pushed-out surfaces of TRISO-coated model tubes: (a) and (b) thin specimen (118 μm), (c) and (d) thick specimen (279 μm).

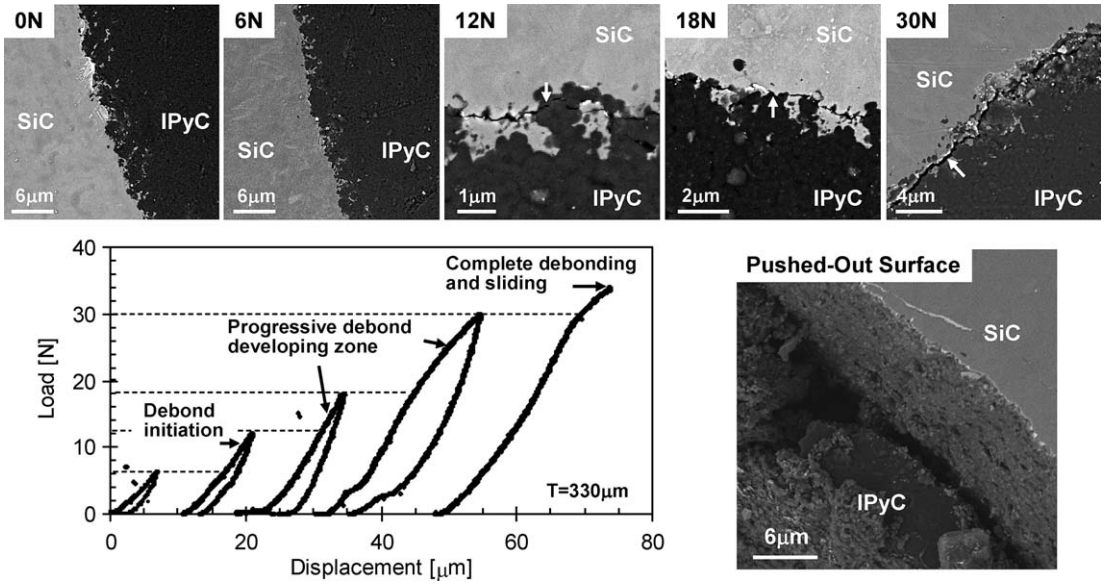


Fig. 7. Extracted loading/unloading curves during push-out test and corresponding surface images in each sequence.

sliding surfaces in the debonded region. Progressive debonding continues as long as the applied load exceeds the value of the forces associated with interfacial debonding and frictional sliding up to the

peak load, which is followed by a sudden load drop. This load drop indicates the occurrence of complete debonding of the interface. For thin test specimens, both debonding and complete sliding occurred simultaneously at the maximum load.

A plateau in the load–displacement curve indicates frictional equilibrium during sliding at the IPyC/SiC interface, followed by a second load drop. As discussed in the following, the SiC layer of most test specimens were cracked by the contact of the sides of the indenter tip for large push-out displacements (Fig. 6). This observation is supported by the fact that such cracks were never observed for loads below the maximum load value (Fig. 7). The second load drop beyond the plateau thus indicates the fracture of the SiC layer.

Figs. 8–10 summarize experimental data of the debond initiation load, $P_d$, the maximum load, $P_{max}$, and the plateau load, $P_{plateau}$, with respect to the sample thickness $t$. Error bars in each figure correspond to $\pm 1$ standard deviation about the mean value. Reduced fiber push-out data are also listed in Table 2. The debond initiation load is considered to be valid through the entire specimen thickness range tested. The debond initiation load increases monotonically with increasing sample thickness and finally approaches a constant value of ~13 N as the sample thickness becomes larger than 200 μm. In contrast, the maximum load increases exponentially with increasing sample thickness up to 220 μm (Region I). Above a sample thickness of 220 μm (Region II), the maximum load became nearly constant (25–30 N). As discussed, most specimens with a thickness over 220 μm failed by shear deformation due to the intrinsically weak shear strength of PyC. The shear deformation increased the indenter tip end displacement, resulting in cracking of the SiC layer by contact with the sides of the indenter. The actual maximum load was therefore substantially lower than the expected value in Region II. It was not possible to observe a plateau beyond the maximum load for thick specimens with shear failure of the PyC layer. In the analysis of plateau loads, experimental data in Region II were therefore excluded. The plateau load was found to increase with increasing sample thickness (Fig. 10).

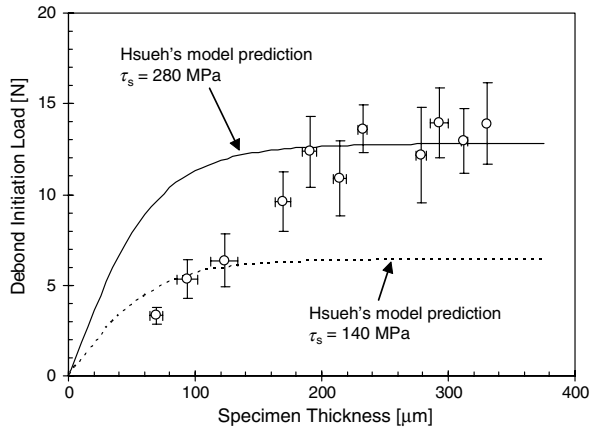


Fig. 8. Debond initiation load versus specimen thickness. Hsueh's model [19] yields an intrinsic interfacial debond shear strength of ~280 MPa for the TRISO-coated specimens.

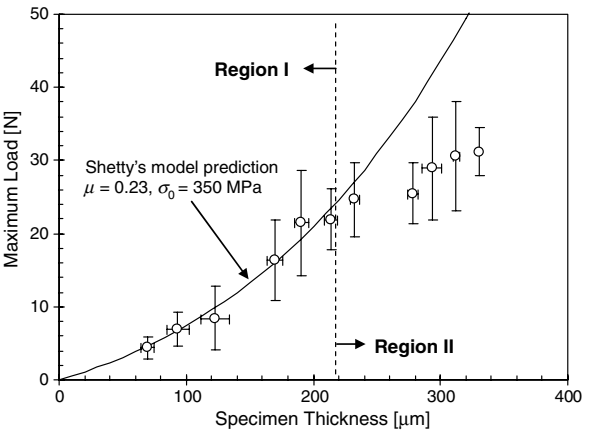


Fig. 9. Maximum push-out load versus specimen thickness. Shetty's model [24] was fitted to data in region I, yielding $\mu = 0.23$ and $\sigma_0 = 350$ MPa. Experimental data in region II were not considered in the analysis because thick TRISO-coated model tubes accompanied with degradation of the inner pyrolytic carbon during push-out test.

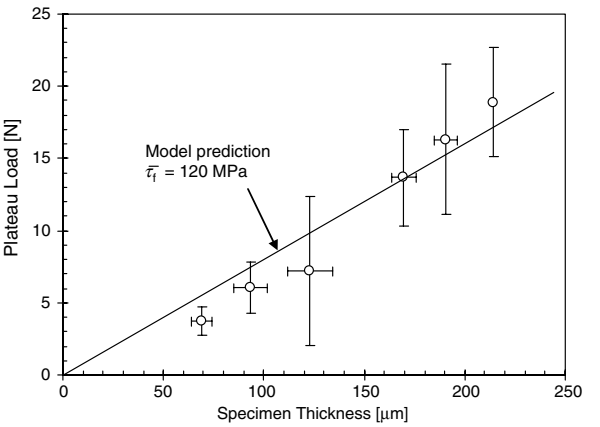


Fig. 10. Plateau load versus specimen thickness. Model fitting provides an average interfacial friction stress of ~120 MPa.

Table 2
Interfacial shear properties of the TRISO-coated model tube

| Sample thickness (μm) | Debond initiation load (N) | Maximum push-out load (N) | Plateau load (N) | Number of tests |
|---|---|---|---|---|
| 69 (8) | 3.3 (0.5) | 4.4 (1.5) | 3.7 (1.0) | 5 |
| 94 (5) | 5.4 (1.1) | 6.9 (2.3) | 6.0 (1.8) | 11 |
| 123 (8) | 6.4 (1.4) | 8.5 (4.4) | 7.2 (5.1) | 4 |
| 170 (11) | 9.6 (1.6) | 16.4 (5.5) | 13.7 (3.4) | 3 |
| 191 (6) | 12.4 (2.0) | 21.5 (7.2) | 16.3 (5.2) | 5 |
| 214 (6) | 10.9 (2.1) | 22.0 (4.2) | 18.9 (3.8) | 5 |
| 232 (5) | 13.6 (1.3) | 24.7 (5.1) | – | 5 |
| 279 (3) | 12.2 (2.6) | 25.5 (4.2) | – | 8 |
| 293 (4) | 13.9 (1.9) | 28.9 (7.1) | – | 7 |
| 312 (7) | 12.9 (1.8) | 30.6 (7.4) | – | 3 |
| 331 (3) | 13.9 (2.3) | 31.2 (3.3) | – | 6 |

Numbers in parenthesis indicate one standard deviation.

### 3.2. Interfacial debond shear strength

The condition of interfacial debonding during push-out has been defined using two criteria: the shear strength criterion [17–19] and the critical energy release rate criterion [20–23]. In the strength-based approach, which is adopted in this study, it is assumed that interfacial debonding occurs when the maximum interfacial shear stress reaches the interfacial shear strength. For the strength criterion, the non-linear shear-lag model is used to analyze the interfacial debond shear strength, $\tau_s$, from debond initiation stress, $\sigma_d$, considering the effect of Poisson's expansion. Note that the debond initiation stress is defined as the debond initiation load divided by the fiber cross-sectional area. The Hsueh model [19], which considers the following precise interactions at the interface: (i) the radial dependence of the axial stresses in both the fiber and the matrix, (ii) the shear stress distribution in the matrix, and (iii) the exact equilibrium equation in relating the tangential stress to the radial stress at the interface, was applied in this study. The Hsueh model is given by [19]

$$\sigma_d = \tau_s \left( \left\{ \frac{r_m^2(1+\nu_m)}{r_m^2 - r_f^2} \left[ \frac{4r_m^2}{r_f^2} \ln\left(\frac{r_m}{r_f}\right) - \frac{(r_m^2 - r_f^2)(3r_m^2 - r_f^2)}{r_f^2 r_m^2} \right] + \frac{r_m^2 - r_f^2}{r_f^2} \left[ \frac{(1+\nu_f)P_1 E_m}{E_f} + 2P_2 \right] \right\} \times \left[ 1 + \frac{r_m^2 - r_f^2}{r_f^2} \left( \frac{P_1 E_m}{E_f} - P_3 \right) \right] \right)^{1/2} \Bigg/ \left\{ \frac{(r_m^2 - r_f^2)P_1 E_m}{r_f^2 E_f \tanh(\alpha t)} + \left[ 1 - \frac{(r_m^2 - r_f^2)P_3}{r_f^2} \right] \left[ \frac{2}{\exp(\alpha t) - \exp(-\alpha t)} \right] \right\}, \quad (1)$$

where $P_1$, $P_2$, $P_3$ and $\alpha$ are constants defined by Young's modulus, $E$, Poisson's ratio, $\nu$, and radius, $r$, of the constituents, subscripts 'f' and 'm' denote the fiber core and the matrix, respectively.

The experimental trend of the compressive load at debond initiation is shown in Fig. 8. By applying Eq. (1), we finally obtain the estimated interfacial debond shear strength of TRISO-coated model tubes (solid and broken curves in Fig. 8). In this study, the multi-layered core is assumed to be isotropic, following the rule of mixtures, since there is no exact solution for multi-layered tubes. The properties of fiber core composed of SCS-9A™ SiC fiber coated by BPyC and IPyC, and SiC matrix of the TRISO-coating are summarized in Table 1. The interfacial debond shear strength exhibits size dependency; approaching a constant value of ~280 MPa with increasing sample thickness.

### 3.3. Interfacial friction stress

Shetty [24] has analyzed the frictional sliding problem using the non-linear shear-lag approach and derived an equation that relates the maximum sliding load after complete debonding and the sample thickness. The complete debonding stress, $P_{max}$, is described as a function of the compressive clamping stress, $\sigma_0$, which is defined to be the summation of the thermally induced residual stress and the

roughness-induced clamping stress, and the friction coefficient, $\mu$

$$P_{\max} = \frac{\pi r_f^2 \sigma_0}{k}\left[\exp\left(\frac{2\mu k t}{r_f}\right) - 1\right], \quad (2)$$

where

$$k = \frac{E_m v_f}{E_f(1+v_m)}. \quad (3)$$

Intrinsic interfacial friction stress, $\tau_f$, is calculated by

$$\tau_f = \mu\sigma_0. \quad (4)$$

The analysis is independent of the shape of the indentation curve; therefore it can also be applied to composites with strong interfacial bonds. Bright et al. [13] applied Shetty's original equation to several composite systems with success in estimating the frictional sliding parameters: residual clamping stress, friction coefficient, and interfacial friction stress. By fitting this equation to the experimental data in Region I (Fig. 9), a residual clamping stress of ~350 MPa and a friction coefficient of ~0.23 were obtained, yielding an intrinsic interfacial friction stress of ~80 MPa.

The average interfacial friction stress, $\bar{\tau}$, is estimated from the plateau stress, $\sigma_{\text{plateau}}$ [11]

$$\bar{\tau} = \frac{\sigma_{\text{plateau}} r_f}{2t}. \quad (5)$$

Therefore the average interfacial frictional stress can be estimated from the ratio of the plateau stress to the sample thickness in Fig. 10. The average interfacial frictional stresses from the plateau load is slightly higher (~120 MPa) than those predicted by Shetty's model (~80 MPa).

## 4. Discussion

### 4.1. Radial cracks in SiC

The pushed-out surfaces (Fig. 6) were accompanied by several radial cracks in the SiC layer, while no cracking was produced in the SiC layer even at the maximum load (Fig. 7). Possible crack initiation mechanisms are suggested: (i) misalignment induced crack initiation, (ii) failure by internal pressurization, (iii) unstable crack propagation at the complete debonding and sliding due to exceptionally strong interfacial strength, and (iv) physical contact with the loading indenter tip.

Polishing often gave poor parallelism of the specimen surfaces. Misalignment of the fiber core causes an anisotropic stress field along the IPyC/SiC interface, probably producing the undesired cracks in the radial direction. Such cracks led to the rapid load drop during push-out tests and did not exhibit a frictional plateau. This type of fracture pattern was not included in the analysis of this study.

Once the fiber core debonds, the outer SiC layer is subjected mostly to the internal pressurization induced by Poisson's expansion and cracked-plane surface roughness. As discussed below, the effect of the thermally induced residual stress was very small for the debonded interface. The calculated hoop stress induced by Poisson's expansion using the complete debonding load becomes less than 100 MPa in the sample thickness range tested. In addition, the very huge radial clamping stress (~350 MPa) primarily due to the rough surface of the cracked-plane may cause a large hoop stress in the SiC layer. Data obtained from the internal pressurization for thin wall SiC cylinders and the study on the specimen size effect [39] suggest that the hoop strength of the tubular model fuel was more than 580 MPa. The failure of a SiC layer by internal pressurization therefore seems unlikely. The presence of the frictional plateau beyond complete debonding may suggest that the failure by internal pressurization was very scarce.

Unstable crack propagation is a likely mechanism to induce radial cracks in the SiC layer. An inherently strong interface and a rough fracture surface might produce crack penetration or deflection into the SiC layer as shown in Fig. 4. However, once cracks propagate to the SiC side, the TRISO-coated model tube no longer sustains any load. Whenever this type of fracture occurred, a large load drop would be observed. In this study, such data were considered invalid.

The most likely failure mechanism of the SiC layer is a physical contact with the indenter tip after complete sliding. The indenter end displacement can significantly increase when the strain energy stored in the test system is released by the occurrence of complete sliding. That is the reason for very limited frictional equilibrium after the complete debonding. Specifically, the thick specimens require large loads for complete debonding, hence the magnitude of the strain release must be significantly large. Moreover, specimens with IPyC degradation could enhance the indenter tip end displacement and the indenter sidewall could contact the outer SiC layer (generating a

radial pressure) before the applied load reached potential complete debonding load. Neither the maximum load nor the plateau load is defined in this type of fracture.

### 4.2. Interfacial debond shear strength

The interfacial debond shear strength of the TRISO-coating exhibits size dependence; it increases with increasing sample thickness and approaches a constant value for sample thickness above 220 μm. In the model prediction, the interfacial shear stress is assumed uniform along the entire interface for simplicity. However, the uniform shear stress distribution might not be established near the free surface due to enhanced stress relieving, resulting in decreasing shear stress near the specimen surfaces. Specifically, this effect may be significant for the very thin specimens. Therefore, the intrinsic interfacial debond shear strength can be estimated by the value obtained for the sufficiently thick specimens.

In the conventional SiC/SiC composite system: Nicalon™ SiC fiber reinforced chemically vapor infiltrated (CVI) SiC matrix composites with single-layered PyC interphase [11], which is often referred to discuss the interfacial shear properties of the PyC/SiC interface, a critical crack initiated along the interface between the Nicalon™ fiber and the PyC interlayer. The magnitude of the interfacial debond shear strength between the Nicalon™ fiber and the PyC interface was approximately 170–200 MPa. It was concluded that the weaker bonding strength at the Nicalon™/PyC interface was attributed to the weak bonding between amorphous silica, which is generally formed on the surface of the Nicalon™ fiber due to process-induced impurity, and the PyC coating. In contrast, the highly pure and crystalline characteristics of the PyC and the SiC form a pure PyC/SiC interface, providing relatively strong interfacial strength. The interfacial debond shear strength of the TRISO-coated model tubes (~280 MPa) was therefore relatively higher than that of the Nicalon™/PyC interface.

### 4.3. Effects of thermally induced residual stress and interfacial roughness

The clamping stress is, in general, calculated by contributions of residual radial stresses induced by the mismatch of coefficients of thermal expansion (CTE) between the PyC and the SiC, and by surface roughness at the cracked-plane. The analytical solutions for the residual stress arising from the CTE mismatch, $\sigma_{CTE}$, are developed by Oel and Frechette [40] and Mikata and Taya [41]. These analytical models can be simply extended to a multi-layered tubular material. Fig. 11 shows a relationship between the residual radial stress and the radial distance from a core center. As inferred from the figure, the small difference of CTE between the IPyC ($3.5–5.1 \times 10^{-6}$/°C) [35] and the SiC ($\sim 4.0 \times 10^{-6}$/°C) [36] limited the CTE mismatch-induced tensile clamping stress (~70 MPa) at the IPyC/SiC interface of the TRISO-coated model tubes. Specifically, for the debonded interface, the residual tensile stress does not contribute as a clamping mechanism. This suggests that the effect of the thermally induced clamping stress was very minor for the TRISO-coated model tubes.

In contrast, the roughness-induced radial stress, $\sigma_R$, is proposed by Kerans and Parthasarathy [25]. The IPyC surface with the crystallite size of <100 nm provides a roughness-induced clamping stress of at most 50 MPa. However, the crack surface obtained from the micrographs (Fig. 5) was more tortuous, producing a rough surface with the magnitude of several hundred nanometers. The rough surface of the actual crack path can provide a larger clamping stress. A roughness-induced clamping stress of ~300 MPa can be estimated.

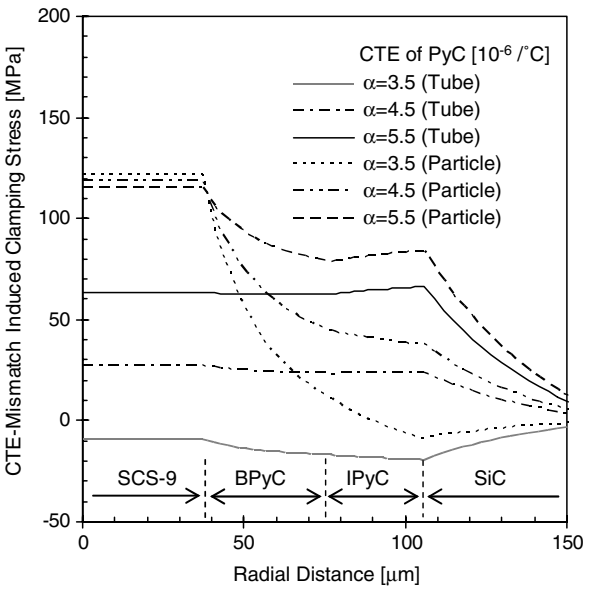


Fig. 11. Calculated residual radial stress distributions of TRISO-coated model tubes and TRISO-coated particles.

The residual clamping stress of the TRISO-coated model tubes (~350 MPa) is a little lower than that of Nicalon™/PyC/CVI-SiC composite (460–760 MPa). The low CTE of the Nicalon™ fiber relative to the matrix yields a small amount of $\sigma_{CTE}$ (~180 MPa) with the largest contribution of the clamping stress coming from roughness-induced radial stress [11]. Even when the magnitude of the fiber surface roughness (~35 nm) is small, large values of roughness-induced radial stress (280–580 MPa) can be generated at the interface. The significantly large difference in contribution of the surface roughness is primarily attributed to the Young's modulus: ~270 GPa for the Nicalon™ fiber versus ~66 GPa for the TRISO fiber core.

Fiber roughness also has a significant influence on the friction coefficient. Generally, the rougher surface provides a higher frictional stress at the interface. The surface of Nicalon™ fiber is inherently smooth, resulting in a small friction coefficient, ~0.03 [11,14]. Utilization of the Nicalon™ fiber with strong debonding surface by surface treatment [11] or the highly crystalline SiC fibers, Hi-Nicalon™ Type-S and Tyranno™-SA [42], makes a remarkable improvement of the frictional shear during sliding. A thin carbon interphase also maximizes the friction due to the enhanced effect of roughness of the SiC matrix [14]. It logically follows that the order of higher magnitude surface roughness of the TRISO-coating results in a significantly higher friction coefficient (~0.23).

The combination of the high clamping stress and coefficient of friction consequently yields a large frictional stress, ~80 MPa. The frictional stress estimated from the plateau load exhibits slightly larger (~120 MPa) than the result from analytical prediction in the sample thickness range. The large frictional stress is probably explained by the presence of debris induced by wearing during sliding.

### 4.4. Interfacial shear properties of TRISO-coated fuel particles

The microstructure of IPyC/SiC interface for the model tubes of this study is identical to the TRISO-coated fuel particles and hence TRISO-coated fuel particles should exhibit a similar crack surface after debonding. This may support no significant change of the friction coefficient between the tube and the particle. In contrast, the internal stress state will be different in each specimen type due to the different geometry. This difference may impact the thermally induced residual stress and roughness-induced clamping stress, both of which determine the magnitude of frictional shear stress at the IPyC/SiC interface.

Fig. 11 also shows an estimate of thermally induced residual stress of TRISO-coated model particles. The layer thicknesses of TRISO-coated model particles are assumed same with TRISO-coated model tubes tested in this study. In a spherical model, thermally induced residual radial stress at the IPyC/SiC interface becomes slightly more tensile than that of TRISO-coated model tubes. However, the very small difference of residual radial stress of 10–20 MPa would not cause a substantial change of frictional shear stress. The majority of frictional shear stress is therefore derived from roughness of the cracked-plane. The roughness-induced clamping stress still remains large even for a spherical material.

The effect of CTE mismatch-induced residual stress on interfacial debond shear strength is also minor, although it may exist. Therefore, the interfacial debond shear strength of TRISO-coated fuel particles can be estimated from the intrinsic value determined in Fig. 8 for the thick specimens.

## 5. Conclusions

In order to evaluate interfacial shear properties at the IPyC/SiC interface of the TRISO-coated model tube, a micro-indentation push-out test, originally developed for continuous fiber reinforced ceramic matrix composites, was applied. Major findings are as follows:

(1) The micro-indentation push-out test system using a flat-bottom indenter tip and a high load capacity was successfully applied to evaluation of interfacial shear properties for the TRISO-coated model tubular specimen. Existing non-linear shear-lag models provide reasonable prediction of the interfacial debond shear strength and the interfacial frictional stress of the IPyC/SiC interface.
(2) The push-out process was very similar to that of the conventional SiC/SiC composites: (i) debond initiation at the IPyC/SiC interface beyond the proportional limit of the initial linear elastic deformation, (ii) crack development along the IPyC/SiC interface and incorporated sliding friction, (iii) complete debonding and sliding at the maximum load, (iv) frictional shear load transfer via the pushed-out

fiber surface, (v) equilibrium of the frictional shear load with the applied compressive load.

(3) Interfacial debond shear strength had a size dependency; it tended to increase with increasing sample thickness and approached a constant value. The intrinsic interfacial debond shear strength of ~280 MPa was estimated.
(4) High residual clamping stress (~350 MPa) and friction coefficient (~0.23) of TRISO-coated model tubes were primarily due to the rough-surfaced crack path, yielding a relatively large interfacial frictional stress (~80 MPa).
(5) Preliminary test results indicate that the rough estimation of interfacial shear properties of TRISO-coated fuel particles is in good agreement with those of TRISO-coated model tubes.

## Acknowledgements

The authors would like to thank Dr T.S. Byun for micro-indentation push-out testing. Thanks are extended to Drs T.S. Byun and S.J. Zinkle for reviewing the manuscript. This research was sponsored by the US Department of Energy Office of Nuclear Energy, Science and Technology, a Nuclear Energy Research Initiative (NERI) Project, under contract NEAF355 (AF3510) with Oak Ridge National Laboratory (operated by UT-Battelle, LLC).

## References

[1] A technology roadmap for generation IV nuclear energy systems, US DOE Nuclear Energy Research Advisory Committee and the Generation IV International Forum, 2002.
[2] L. Wolf, G. Ballensiefen, W. Fröhling, Nucl. Eng. Des. 34 (1975) 93.
[3] T.D. Gulden, H. Nickel, Nucl. Technol. 35 (1977) 206.
[4] D.A. Petti, J. Buongiorno, J.T. Maki, R.R. Hobbins, G.K. Miller, Nucl. Eng. Des. 222 (2003) 281.
[5] G.K. Miller, D.A. Petti, D.J. Varacalle Jr., J.T. Maki, J. Nucl. Mater. 317 (2003) 69.
[6] G.K. Miller, D.A. Petti, J.T. Maki, J. Nucl. Mater. 334 (2004) 79.
[7] J. Lamon, F. Rebillat, A.G. Evans, J. Am. Ceram. Soc. 78 (1995) 401.
[8] D.B. Marshall, W.C. Oliver, J. Am. Ceram. Soc. 70 (1987) 542.
[9] C.-H. Hsueh, J. Am. Ceram. Soc. 76 (1993) 3041.
[10] E. Lara-Curzio, M.K. Ferber, J. Mater. Sci. 29 (1994) 6152.
[11] F. Rebillat, J. Lamon, R. Naslain, E. Lara-Curzio, M.K. Ferber, T.M. Besmann, J. Am. Ceram. Soc. 81 (1998) 965.
[12] W.A. Curtin, J.I. Eldridge, G.V. Srinivasan, J. Am. Ceram. Soc. 76 (1993) 2300.
[13] J.D. Bright, D.K. Shetty, C.W. Griffin, S.Y. Limaye, J. Am. Ceram. Soc. 72 (1989) 1891.
[14] E. Lara-Curzio, M.K. Ferber, R.A. Lowden, Ceram. Eng. Sci. Proc. 15 (1994) 989.
[15] D.H. Grande, J.F. Mandell, K.C.C. Hong, J. Mater. Sci. 23 (1988) 311.
[16] C.G. Cofer, J. Economy, M.K. Ferber, E. Lara-Curzio, Ceram. Eng. Sci. Proc. 15 (1994) 447.
[17] P. Lawrence, J. Mater. Sci. 7 (1972) 1.
[18] A. Takaku, R.G.C. Arridge, J. Phys. D 6 (1973) 2038.
[19] C.-H. Hsueh, Mater. Sci. Eng. A 154 (1992) 125.
[20] C. Gurney, J. Hunt, Proc. Roy. Soc. London, Ser. A 299 (1967) 508.
[21] H. Stang, S.P. Shah, J. Mater. Sci. 21 (1986) 953.
[22] Y.C. Gao, Y.W. Mai, B. Cotterell, J. Appl. Math. Phys. 39 (1988) 550.
[23] C.-H. Hsueh, Mater. Sci. Eng. A 159 (1992) 65.
[24] D.K. Shetty, J. Am. Ceram. Soc. 71 (1988) C107.
[25] R.J. Kerans, T.A. Parthasarathy, J. Am. Ceram. Soc. 74 (1991) 1585.
[26] C. Liang, J.W. Hutchinson, Mech. Mater. 14 (1993) 207.
[27] J.L. Kaae, J. Nucl. Mater. 29 (1969) 249.
[28] J.L. Kaae, J. Nucl. Mater. 32 (1969) 322.
[29] J.L. Kaae, J. Nucl. Mater. 46 (1973) 121.
[30] R.J. Price, J.C. Bokros, J. Nucl. Mater. 21 (1967) 158.
[31] W.C. Oliver, G.M. Pharr, J. Mater. Res. 7 (1992) 1564.
[32] Product sheet from Specialty Materials Inc., Lowell, MA.
[33] J.L. Kaae, Carbon 9 (1971) 291.
[34] R.J. Price, J.L. Kaae, Carbon 7 (1969) 706.
[35] R.J. Price, J.C. Bokros, K. Koyama, Carbon 5 (1967) 423.
[36] Product sheet from Rohm and Haas Company Advanced Materials, Woburn, MA.
[37] R.J. Price, Nucl. Technol. 35 (1977) 320.
[38] B.O. Yavuz, R.E. Tressler, Ceram. Inter. 8 (1992) 19.
[39] L.L. Snead, T.S. Byun, Y. Katoh, T. Nozawa, R.A. Lowden, J.H. Miller, NEAF-940 Coated fuel particles progress report, vol. 11, 2005, p. 7.
[40] H.J. Oel, V.D. Frechette, J. Am. Ceram. Soc. 69 (1986) 342.
[41] Y. Mikata, M. Taya, J. Compos. Mater. 19 (1985) 554.
[42] W. Yang, A. Kohyama, T. Noda, Y. Katoh, T. Hinoki, H. Araki, J. Yu, J. Nucl. Mater. 307–311 (2002) 1088.